# Instructions to Authors for the Preparation of Papers for the 17th Australian International Aerospace Congress

*Please select category below:*
Normal Paper ☐
Student Paper ☒
Young Engineer Paper ☐

# Modelling of Defective Bearings – The importance of the leading and trailing edge angle of a defect

Francesco Larizza [1*], Carl Q. Howard [1], Steven Grainger [1] and Wenyi Wang[2]

[1] *School of Mechanical Engineering, University of Adelaide, SA 5005*
[2] *Aerospace Division DST Group,*
*506 Lorimer Street, Fishermans Bend, Victoria, 3207, Australia*
*\* francesco.larizza@adelaide.edu.au*

## Abstract

Rolling element bearings eventually become worn and develop surface defects, such as spalls, dents, and pits. Researchers have tested bearings with sharp 90° rectangular edges to develop methods to estimate the size of a defect. However, these idealised rectangular defects do not occur in the real world. An analytical model has been developed for a cylindrical roller bearing with a defect that has sloped leading and trailing edges on the outer raceway. The results from the simulations were compared with experimental results. It was found that the vibration signatures of the entry and exit events are still detectable and have similar characteristics to those that are generated in bearings with sharp-edged rectangular defects, and the predicted vibration response can accurately predict these vibration signatures.

**Keywords:** Rolling element bearing, Spall, Defect size, Contact forces, Vibration model

## 1. Introduction

Bearings in a machine will eventually fail, and the most common reason for failure are the formation of surface defects from the propagation of fatigue cracks or the removal of surface grains during operation. These defects occur due to insufficient lubrication and high contact stresses between the rolling element and the raceway of the bearing, causing spalls, dents, and pits to form on the contact surfaces. These defects cause the applied load on the rolling element to differ, making the relative distance from the inner ring to the outer ring vary from normal, resulting in higher than normal vibration amplitudes. The condition of a defective bearing can be determined by analysing this vibration response, which can be used for scheduling maintenance actions.

Previous studies on the vibration signature of a bearing with a sharp rectangular defect found that as the rolling element traverses the defect the resultant vibration response has two distinct features. The first is a low-frequency component that is caused by the rolling element entering the defect and the second is a high-frequency component, which is caused by the rolling element striking the trailing edge of the defect [1, 2, 3, 4].

*Tenth DST Group International Conference on Health and Usage Monitoring Systems*
*17ᵗʰ Australian Aerospace Congress, 26-28 February 2017, Melbourne*

This study investigated the effects of an angled entry and exit profile on the vibration response of a defective bearing with a spall defect and presents an updated model that was used to predict the vibration response of the defective bearing and to calculate the contact forces rolling elements and the raceway rough surfaces.

## 2. Previous Work

Previous researchers have examined the vibration response resulting from sharp rectangular defects that have a 90° angle from the bottom of the defect to the leading and trailing edges [2, 5, 6, 7, 1]. The measured vibration response that is generated by this type of defect is presented in Figure 1.
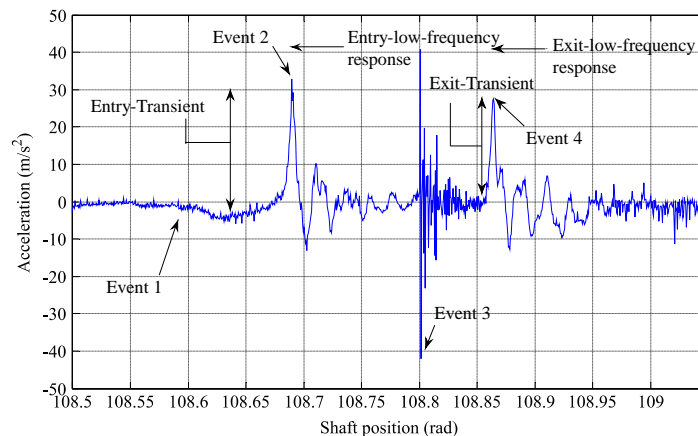


*Figure 1. The vibration response of a bearing as a rolling element travels through a rectangular spall defect on the outer ring, showing the low and high-frequency events. Image adapted from Moazen-Ahmadi et al [1].*

Previous experimental and simulation studies by Moazen-Ahmadi et al [2] and Singh et al [3] showed that the decrease in the acceleration occurs when the roller begins to transition into the defect (Event-1), and when the rolling element has completely unloaded a low-frequency response occurs (Event-2). It was also suggested that the high-frequency event is a resultant of the rolling element striking the trailing edge of the defect; or for a defect with a large circumferential extent when the rolling element strikes the bottom of the defect (Event-3). A second low-frequency event occurs as the rolling element begins to reload between the raceways, as it exits the defect (Event-4). Figure 1 highlights events 1 to 4. By using the time between the two low-frequency events and the change in relative distance between the inner and outer rings, Moazen-Ahmadi et al [1], developed a method for estimating the defect size that was more accurate than the method presented by Sawalhi and Randall [7].

Numerous multi-body dynamic model have been developed to understand the relationship between the vibration response and the path of the rolling element, as it traverses through a line spall [2, 3, 5, 4, 8, 9]. There has been some research conducted that have experimentally measured the path of a rolling element using a derotator or a dove lens. However, the resolution of these results are not sufficient to verify this part of the model. To simplify the analysis, the majority of the multi-body models included a combination of the following assumptions:
1. The outer and inner rings are rigid, and the rings are rigidly connected to the housing and shaft [5, 4, 8, 9]
2. The rolling elements are excluded or considered massless points [5, 4, 8, 9]
3. The rolling element path is assumed [5, 4, 8, 9]

*Tenth DST Group International Conference on Health and Usage Monitoring Systems*
*17th Australian Aerospace Congress, 26-28 February 2017, Melbourne*

4. Inertia and centripetal forces acting on the rolling elements are ignored [5, 4, 8, 9]
5. Slippage of the rolling elements are ignored [2, 5, 8, 9]
6. The elasto-hydraulic lubrication fluid film is ignored [2, 3, 4, 5, 8, 9]

Moazen-Ahmadi et al. [2] developed a comprehensive model, where the rolling elements are considered to have finite mass and size; and the path of the roller is not pre-defined but determined through appropriate physics, such as centripetal acceleration and the change in the contact point as the rolling element transitions into the defect. However, as a means to develop new defect size estimation methods and to predict the remaining life of a damaged bearing, the model has limitations, such as the wavelength of the roughness and the circumferential defect length must be larger than the circumferential contact length. These limitations are a result of the model using Hertzian contact theory to determine the contact forces, which require that the contact surfaces be smooth and continuous. Therefore, when calculating the contact forces on a rough surface or a surface where the curvature changes rapidly, Hertzian contact theory should not be used. The reason is that when a rolling element enters a defect, the circumferential contact length becomes skewed from the point of maximum deformation as it reaches the leading edge of the defect; and with a rough surface the contact patch is no longer a rectangle, as points may not be in contact with the raceway. The method used to overcome this limitation is discussed in Section 4.

## 3. Experimental Method

The test cases consisted of two defective bearings with an applied load of 5 kN and a shaft speed of 5 Hz. Both bearings were Electric Discharge Machined (EDM) to 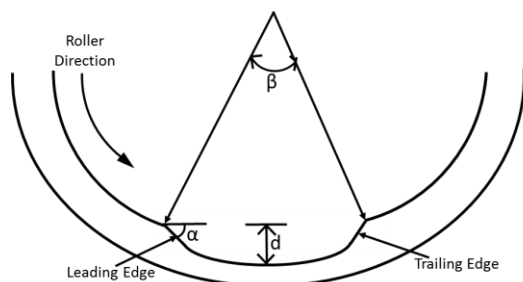have a normally cross-section profile that, is shown in Figure 2. Diagram of the defect profile showing the controlled defect parameters. Where, α is the leading and trailing edge slope, β is the arc angle of the defect and d is the maximum depth of the defect. Test bearing 1 had a 90° sloped leading and trailing edge and test bearing 2 had a 5° sloped leading and trailing edge, both bearings were a FAG N206E.TVP2. Before conducting the tests, each bearing was worn in for 30 minutes to ensure that the dynamic response would not change over time, due to deformations of the leading and trailing edges.



*Figure 2. Diagram of the defect profile showing the controlled defect parameters. Where, α is the leading and trailing edge slope, β is the arc angle of the defect and d is the maximum depth of the defect.*
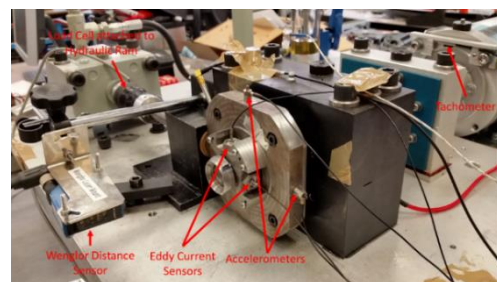


*Figure 3. Photo of the bearing test rig used to capture the vibration response of the defective bearings.*

Figure 3, shows the test rig used that was used to capture the dynamic response of the defective bearings. The load was applied using a hydraulic piston, and a load cell placed in series was used to measure the applied load. A tachometer was used to measure the shaft speed. A laser distance (Wenglor CP24MHT80) sensor was used to create a trigger signal when a rolling element entered the defect and as a tachometer to determine the cage speed. The test bearing housing was a floating housing with two stud-mounted accelerometers mounted on the housing in the x and y-directions, to measure the vibrations induced by the defect. Two eddy current proximity probes (Micro-Epsilon EP05-C3) were mounted in the x

and y-direction to measure the change of the relative distance between the inner and outer rings. Figure 3 shows the positions of the accelerometers and the displacement sensors used in the experiments. The data was captured using a National Instruments cDAQ modules (NI 9234) at a sampling rate of 25.6 kHz, and was processed using Matlab.

## 4. Bearing Contact Model

As discussed in Section 2, a limitation of the model presented by Moazen-Ahmadi et al. [2], is that the defect length and the roughness wavelength of the surface must be larger than the contact length. Therefore, the model cannot accurately determine the contact force and the contact area when a rolling element encounters a rough surface, a single pit defect or multiple pit defects on the contact surface. The proposed nonlinear multi-body dynamic model is is an extension of the model developed by Moazen-Ahmadi et al. [2]; and this paper will only discuss the new methodology for calculating the contact forces and the rigid-body penetration between a smooth rolling element and the raceway.

*3.1 Contact Force Applied to the Rolling Elements*

To remove this limitation, a numerical method that uses Love's equation was used to calculate the contact area and contact force of a smooth rolling element on any surface. The contact model utilised in the newly developed model does not consider plastic deformation, as this will be used in future work to determine the possible growth of a defect and to reduce the computation time of the contact model. Love's equation allows the discretisation of the contact surface into finite elements and the calculation of the contribution an applied pressure on any element has on the deformation of another element. The discretised surface of a flat plane, where the element size is *2a* by *2b* and the rigid body penetration $U_z$ at node *z*. The rigid body penetration of an element is given by

$$
\begin{aligned}
U_z = \sum_{z=1}^{n} \sum_{i=1}^{m} \frac{2p_i(1-v^2)}{\pi E} &\left[ \left( (x+a) \ln\left( \frac{(y+b) + ((y+b)^2 + (x+a)^2)^{\frac{1}{2}}}{(y-b) + ((y-b)^2 + (x+a)^2)^{\frac{1}{2}}} \right) \right) \right. \\
&+ \left( (y+b) \ln\left( \frac{(x+a) + ((y+b)^2 + (x+a)^2)^{\frac{1}{2}}}{(x-a) + ((y+b)^2 + (x-a)^2)^{\frac{1}{2}}} \right) \right) \\
&+ \left( (x-a) \ln\left( \frac{(y-b) + ((y-b)^2 + (x-a)^2)^{\frac{1}{2}}}{(y+b) + ((y+b)^2 + (x-a)^2)^{\frac{1}{2}}} \right) \right) \\
&+ \left. \left( (y-b) \ln\left( \frac{(x-a) + ((y-b)^2 + (x-a)^2)^{\frac{1}{2}}}{(x+a) + ((y-b)^2 + (x+a)^2)^{\frac{1}{2}}} \right) \right) \right],
\end{aligned}
\tag{1}
$$

where *a* is the half element length, *b* is half the element width, *x* and *y* are the distance from node *z* to $p_i$ in the *x* and *y*-direction respectively; $p_i$ is the applied pressure on the element that is contributing to the deformation at *z*; and *v* and *E* are the Poisson's Ratio and the Young's Modulus of the material, respectively. The distances from node *z* to $p_i$ in the *x* and *y*-directions and the rigid body penetration $U_z$ are given by

$$
x = 2a|z_x - i_x|,
\tag{2}
$$

$$
y = 2b|z_y - i_y|,
\tag{3}
$$

$$U_z = \delta(\psi_{max}) - (r - r\cos(\theta_{ro})) - (r_a - r_a\cos(\theta_{ra})) + (Ro(\psi) - Ro(\psi)\cos(\theta_{Ro})) + (Ro(\psi) - Ro(\psi_{max})), (4)$$

where $z_x$ and $z_y$ are the $x$ and $y$-coordinates of node $z$, $i_x$ and $i_y$ are the $x$ and $y$-coordinates of the applied pressure $p_i$, $Ro(\psi)$ is the distance from the centre of the outer ring to the outer raceway, $\delta(\psi)$ is the rigid body penetration at an angular position of $\psi$, $\delta(\psi_{max})$ is the maximum rigid body penetration, $r$ is the radius of the rolling element, $\theta_{ro}$ is the arc angle from the point of maximum rigid body penetration to another node for the rolling element at an angular position of $\psi$, $r_a$ is the axial curvature of the rolling element, $\theta_{ra}$ is the angle from the point of maximum rigid body penetration to $U_z$ and $\theta_{Ro}$ is the arc angle from the point of maximum rigid body penetration to another node on the outer.

The inverse matrix method can be used to solve the system of equations, to determine the applied pressures on the elements. If the calculated applied pressure on an element is negative, then that point is not in contact, as a negative pressure means that element is in. Therefore, the contact width needs to be reduced, and the applied pressures recalculated until the applied pressures are all equal to or greater than zero. For a more in-depth discussion on the contact force methodology, refer to Poon and Sayles [10].

## 5. Results and Discussion

This section presents the measured and the simulated dynamic response for the two defective bearings. The aim is to show how the dynamic response of a faulty bearing changes when there is a smooth transition into and out of the defect, unlike the sharp rectangular defects used in previous research; and to present the capabilities of the new bearing model.

Figure 4 compares the measured vibration response with the predicted vibration response for the two test bearing of the 5° and 90° defect, respectively. Figure 4 (i) compares the change in relative displacement between the inner and outer rings for the measured and predicted responses, and Figure 4 (ii) is the measured acceleration response of the defective bearing. Figure 4 (iii) and (iv) show the predicted acceleration response of the defective bearing and the relative distance the rolling element surface from the outer raceway, respectively.

Using Figure 4 (i) and (ii) key vibration signatures are highlighted 1 through 6, and these points are compared to the angular positions where these events happen in the predicted response:
- Event-1 is the rolling element entering the defect,
- Event-2 is when the rolling element has completely unloaded,
- Event-3 is when the rolling element striking the trailing edge of the defect,
- Event-4 is the when the rolling element begins to reload as it is forced out of the defect,
- Event-5 is the unloaded rolling element inside the defective area hits the outer raceway,
- Event-6 is an unloaded roller outside or inside the defect striking the outer raceway.

From Figure 4, the simulated response can accurately determine the Event-1 through to 6. However, the amplitudes of the predicted responses are slightly overestimated as the damping of the system is a simple constant value that is 3%. In the predicted response the high-frequency acceleration responses Events 5 and 6 do not always align with a rolling element striking the bottom of the defect or the outer raceway, but the model can predict small impacts. This misalignment could be due to the actual defect topography not being known and the effect of the grease in the bearing not being modelled.

The predicted results for the 90° defect align well with Event-1 through to Event-6 with the measured response. When the predicted results are compared to the measured response of the 5° defect the simulation results, align well with Events-1 through to Event-6. However, the estimated slope angle of the leading edge is 2.5° and the trailing edge is 5° for the simulated defect. This difference in the slope of the leading and trailing edge from the simulated and measured defect could be due to the actual defect topography not being known, and future work could be to identify a method to scan the surface topography of the defect.

When the measured change in relative displacement between the rings and band-pass filtered acceleration response during the entry and exit events of the two defective bearings were compared, it was found that the bearing with the 90° transition completely unloads more quickly than the 5° leading edge; and the rolling element in the 90° defect begins to reload sometime after the 5° trailing edge. This is expected due to the shallow angle of the leading and trailing edges, as the rolling element in the sloped defect remains in contact of longer and comes into contact with the trailing edge of the defect before the rolling element in the 90° defect hits its trailing edge, as shown in Figure 5 (i) – (iv).
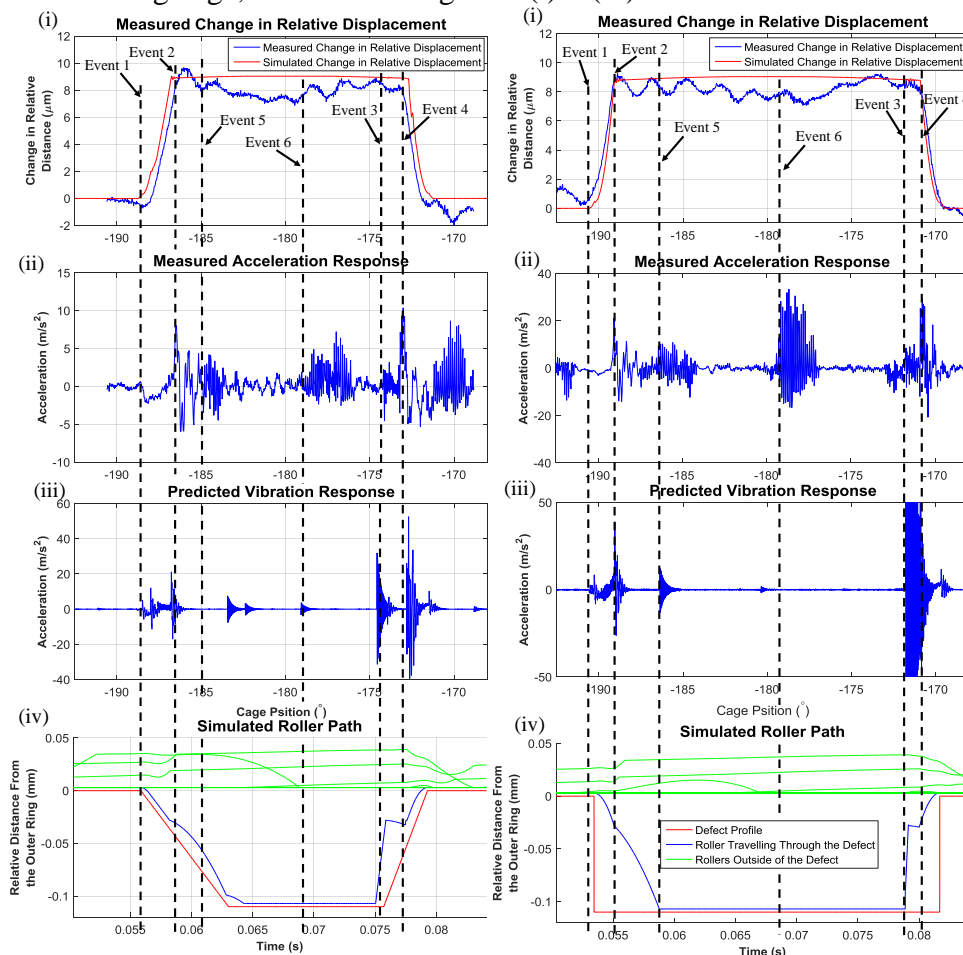


*a) Comparison of the measured signals for a defective bearing with a 5° leading and trailing edge and an arc length of 17° and the simulated dynamic response.*

*b) Comparison of the measured signals for a defective bearing with a 90° leading and trailing edge and a an arclength of 20° and the simulated dynamic response.*

*Figure 2. Comparison of the measured signals with the simulated dynamic response: (i) measured change in relative distance between the inner and outer raceway; and the light gate signal, (ii) measured acceleration signal, (iii) simulated acceleration signal and (iv) the predicted roller path.*
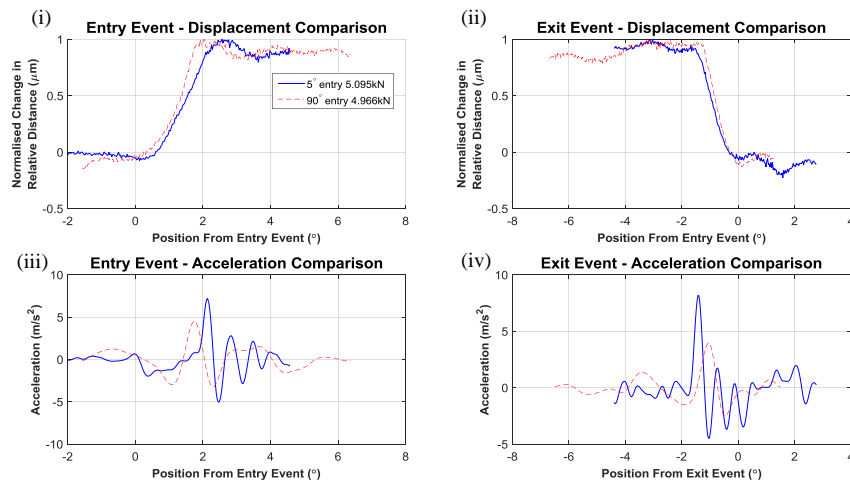
*Figure 3. Comparison of the entry and exit events of the two defective bearings with varying sloped leading and trailing edge. i) and iii) show the comparison of the entry event, where i) is a comparison of the change in relative displacement and iii) is an acceleration comparison. ii) and iv) show the comparison of the exit event, where ii) is a comparison of the change in relative displacement and iv) is an acceleration comparison.*

## 6. Conclusion

This paper has demonstrated the effects the slope of the leading and trailing edge of a spall defect on the vibration response on an operational bearing. The inconsistencies in the assumptions made by previous models about the contact forces between the rolling element and the raceway are presented in this paper. The effects of the sloped leading and trailing edges on the acceleration response and the change in relative displacement between the inner and outer rings were investigated. The path the rolling element takes when traversing through the defect was studied using the predicted rolling element path determined by the new bearing model. Based on the findings from the study, the developed model can determine the path of the rolling elements as it traverses through the defect with a sloped entry and exit edges.

## 7. Acknowledgments

## References

[1] A. Moazen-Ahmadi, C. Q. Howard and D. Petersen, "The path of rolling elements in defective bearings: Observations, analysis and methods to estimate spall size," *Journal of Sound and Vibration,* vol. 366, 2015.

[2] A. Moazen-Ahmadi, D. Petersen and C. Q. Howard, "A nonlinear dynamic vibration model of defective bearings - The importance of modelling the finite size of rolling elements," *Mechanical Systems and Signal Processing,* vol. 53, no. 1, pp. pp. 309-326, 2015.

[3] S. Singh, U. G. Köpke, C. Q. Howard and D. Petersen, "Analyses of contact forces and vibration response for a defective rolling element bearing using an explicit dynamics finite element model," *Journal of Sound and Vibration,* vol. 333, pp. pp. 5356-5377, 2014.

[4] N. Sawalhi and R. B. Randall, "Simulating gear and bearing interactions in the presence of faults: Part I. The combined gear bearing dynamic model and the simulation of localised bearing faults," *Mechanical Systems and Signal Processing,* vol. 22, no. 6, pp.

pp. 1924-1951, 2008.

[5] D. Petersen, C. Q. Howard and Z. Prime, "Varying stiffness and load distributions in defective ball bearings: Analytical formulation and application to defect size estimation," *Journal of Sound and Vibration,* vol. 337, no. 1, pp. pp. 284-300, 2015.

[6] S. Singh, U. Köpke, C. Q. Howard, D. Petersen and D. Rennison, "Impact generating mechanisms in damaged rolling element bearings," *Australian Acoustical Society,* vol. 78, no. 1, pp. pp. 92-97, 2013.

[7] N. Sawalhi and R. B. Randall, "Vibration response of spalled rolling element bearings: observations, simulations and signal processing techniques to track the spall size," *Mechanical Systems and Signal Processing,* vol. 25, pp. pp. 846-870, 2011.

[8] J. Sopaneni and A. Mikkolai, "Dynamic model of a deep-groove ball bearing including localized and distributed defects. Part 1: Theory," *Proceedings of the Institution of Mechanical Engineers, Part K: Journal of Multi-body Dynamics,* vol. 217, pp. pp. 201-211, 2003.

[9] A. Choudhury and N. Tandon, "Vibration response of rolling element bearings in a rotor bearing system to a local defect under radial load," *Journal of Tribology,* vol. 128, pp. pp. 252-261, 2006.

[10] R. S. Sayles and S. Y. Poon, "Surface topography and rolling element vibration," *Precision Engineering,* vol. 3, no. 3, pp. pp. 137-144, 1981.